X-ray Crystal Structure of Aristolochene Synthase from *Aspergillus terreus* and Evolution of Templates for the Cyclization of Farnesyl Diphosphate[†,‡]

Ekaterina Y. Shishova,[§] Luigi Di Costanzo,[§] David E. Cane,[||] and David W. Christianson*[,§]

Roy and Diana Vagelos Laboratories, Department of Chemistry, University of Pennsylvania, Philadelphia, Pennsylvania 19104-6323, and Department of Chemistry, Brown University, Providence, Rhode Island 02912

Received October 31, 2006; Revised Manuscript Received December 18, 2006

ABSTRACT: Aristolochene synthase from *Aspergillus terreus* catalyzes the cyclization of the universal sesquiterpene precursor, farnesyl diphosphate, to form the bicyclic hydrocarbon aristolochene. The 2.2 Å resolution X-ray crystal structure of aristolochene synthase reveals a tetrameric quaternary structure in which each subunit adopts the α-helical class I terpene synthase fold with the active site in the "open", solvent-exposed conformation. Intriguingly, the 2.15 Å resolution crystal structure of the complex with $Mg^{2+}{}_3$-pyrophosphate reveals ligand binding only to tetramer subunit D, which is stabilized in the "closed" conformation required for catalysis. Tetramer assembly may hinder conformational changes required for the transition from the inactive open conformation to the active closed conformation, thereby accounting for the attenuation of catalytic activity with an increase in enzyme concentration. In both conformations, but especially in the closed conformation, the active site contour is highly complementary in shape to that of aristolochene, and a catalytic function is proposed for the pyrophosphate anion based on its orientation with regard to the presumed binding mode of aristolochene. A similar active site contour is conserved in aristolochene synthase from *Penicillium roqueforti* despite the substantial divergent evolution of these two enzymes, while strikingly different active site contours are found in the sesquiterpene cyclases 5-epi-aristolochene synthase and trichodiene synthase. Thus, the terpenoid cyclase active site plays a critical role as a template in binding the flexible polyisoprenoid substrate in the proper conformation for catalysis. Across the greater family of terpenoid cyclases, this template is highly evolvable within a conserved α-helical fold for the synthesis of terpene natural products of diverse structure and stereochemistry.

The terpenoid family consists of tens of thousands of structurally and stereochemically complex natural products that ultimately derive from a mere handful of linear isoprenoid precursors. For example, cyclic sesquiterpenes comprise a broad family of C_{15}-isoprenoids that serve myriad biological functions in plants, bacteria, and fungi (*1*, *2*), yet each sesquiterpene derives from the universal sesquiterpene precursor, farnesyl diphosphate, through a reaction catalyzed by a sesquiterpene cyclase (*2*−*9*). In general, a terpene cyclase governs a specific cyclization cascade with exquisite precision to generate a single, unique product. However, some terpene cyclases are somewhat promiscuous and generate complex mixtures of cyclization products (*10*).

To date, crystal structures of four sesquiterpene cyclases have been determined: 5-epi-aristolochene synthase from *Nicotiana tabacum* (*11*), pentalenene synthase from *Streptomyces* UC5319 (*12*), aristolochene synthase from *Penicillium roqueforti* (*13*), and trichodiene synthase from *Fusarium sporotrichioides* (*14*). Despite the general lack of significant amino acid sequence identity among these cyclases, their three-dimensional structures share a common α-helical fold (*5*, *6*, *9*), as well as two metal binding motifs conserved among monoterpene, sesquiterpene, and diterpene cyclases: the so-called "aspartate−rich" **D**DXX**D/E** motif of helix D (*15*), and the "NSE/DTE" motif (L,V)(V,L,A)(**N,D**)D-(L,I,V)X(**S,T**)XXX**E** of helix H, in which boldface residues are usually magnesium ligands (*14*, *16*). A sesquiterpene cyclase initiates catalysis by the metal ion-dependent ionization of farnesyl diphosphate to generate inorganic pyrophosphate and a highly reactive allylic carbocation.

Aristolochene synthase catalyzes the cyclization of farnesyl diphosphate to form the bicyclic sesquiterpene (+)-aristolochene. The amino acid sequence of the 36 kDa enzyme from *Aspergillus terreus* is 61% identical with that of the 38 kDa aristolochene synthase from *P. roqueforti* (*13*). In *A. terreus* and *P. roqueforti*, aristolochene formation is the first committed step in the biosynthesis of a group of eremophilene toxins and bioregulators such as PR toxin, sporogen-AO 1, phomenone, and bipolaroxin (*16*). Extensive mechanistic studies on both *P. roqueforti* and *A. terreus* enzymes using stereospecifically labeled farnesyl diphosphate, the anomalous substrate 6,7-dihydrofarnesyl diphosphate, a mechanism-based inhibitor, and site-specific mutants (*17*−*21*) support a common cyclization mechanism (Figure

[†] This work was supported by National Institutes of Health Grants GM 56838 (D.W.C.) and GM 30301 (D.E.C.).

[‡] Atomic coordinates of aristolochene synthase from *A. terreus* and its complex with $Mg^{2+}{}_3$-pyrophosphate have been deposited in the Protein Data Bank with as entries 2E4O and 2OA6, respectively.

* To whom correspondence should be addressed: Roy and Diana Vagelos Laboratories, Department of Chemistry, University of Pennsylvania, 231 S. 34th St., Philadelphia, PA 19104-6323. Phone: (215) 898-5714. Fax: (215) 573-2201. E-mail: chris@sas.upenn.edu.

[§] University of Pennsylvania.

[||] Brown University.

10.1021/bi0622524 CCC: $37.00
Published on Web 01/30/2007

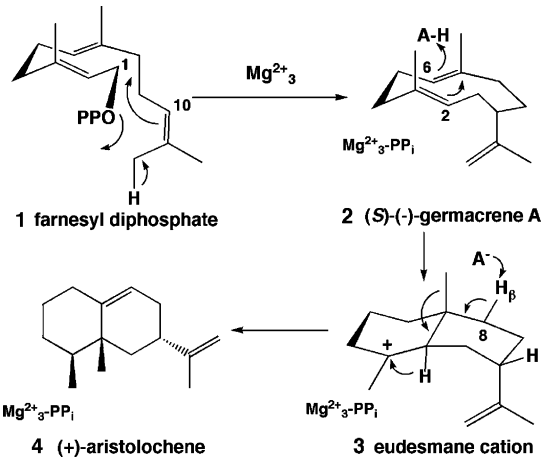

FIGURE 1: Cyclization of farnesyl diphosphate (**1**) to form (+)-aristolochene (**4**). Mechanistic details are summarized in the text; the pyrophosphate leaving group of the substrate may serve as a general acid/general base in catalysis.

1) in which farnesyl diphosphate ionization is accompanied by electrophilic attack on the C10−C11 π bond, with inversion of configuration at C1, resulting in the formation of the neutral hydrocarbon intermediate **2**, (*S*)-(−)-germacrene A. Protonation at C6 and electrophilic attack of the resulting C7 carbocation on the C2−C3 π bond generate the eudesmane cation **3**, which after methyl migration, hydride transfer, and stereospecific deprotonation yields (+)-aristolochene **4**.

Here, we report the X-ray crystal structures of recombinant aristolochene synthase from *A. terreus* at 2.2 Å resolution and its complex with inorganic pyrophosphate (PP_i)[1] and three Mg^{2+} ions at 2.15 Å resolution. Comparison of these structures reveals tertiary structural changes required for catalysis and quaternary structural changes that may attenuate catalytic activity with an increase in enzyme concentration. Moreover, the structural comparison of aristolochene synthases from *A. terreus* and *P. roqueforti* reveals the conservation of a unique active site contour complementary in shape to their common product despite the substantial divergent evolution of these two enzymes. Finally, comparisons of these cyclases with 5-epi-aristolochene synthase and trichodiene synthase reveal striking differences in active site contours, thereby illustrating the biological function of terpene cyclases as both specific and highly evolvable templates for the synthesis of terpene natural products of diverse structure and stereochemistry.

MATERIALS AND METHODS

Recombinant aristolochene synthase from *A. terreus* was expressed at high levels in *Escherichia coli* BL21(DE3)-pLysS (5−10% of total protein) and purified as previously described (*16*) with minor modifications. Briefly, *E. coli* BL21(DE3)pLysS carrying pET11-rASA was inoculated into Luria-Bertani medium containing carbenicillin and grown overnight at 37 °C. A total of 500 mL of LB/carbenicillin medium was inoculated with 5 mL of the overnight seed culture, and *E. coli* was grown at 30 °C until the OD_{600} reached 0.7. Following induction with 0.5 mM isopropyl β-D-thiogalactopyranoside for 4 h, cells were harvested, resuspended in 50 mL of DE52 equilibration buffer [20 mM 2-morpholinoethanesulfonic acid (MES) (pH 6.5), 5 mM ethylenediaminetetraacetic acid, 5 mM β-mercaptoethanol (BME), and 10% glycerol], and sonicated for 10 min using a 50% duty cycle and power range of 30%. After three cycles of sonication, the cell lysate was clarified by centrifugation at 17000*g* and 4 °C for 30 min. The clarified lysate was loaded on DE52 anion exchange resin (80 mL), and a linear gradient from 0 to 500 mM NaCl in cell lysis buffer was applied to elute the enzyme. The most active fractions were pooled, mixed with an equal volume of 3 M ammonium sulfate in DE52 buffer, and applied to a 15 mL methyl HIC column. The enzyme was eluted with a linear gradient from 1.5 to 0 M ammonium sulfate in the same buffer. The most active fractions were desalted on a Sephadex G-25 column and further purified with anion exchange chromatography, using a 10 mL High Q column and a linear gradient from 0 to 300 mM NaCl in DE52 buffer. The resulting protein preparation was 85−90% pure on the basis of SDS−PAGE.

The native enzyme was crystallized by the hanging drop vapor diffusion method at 4 °C. Typically, a 5 μL drop of protein solution [5 mg/mL aristolochene synthase, 25 mM MES (pH 6.5), 2 mM $MgCl_2$, 0.15 M NaCl, and 4 mM BME] was added to 5 μL of precipitant solution [100 mM Tris-HCl (pH 8.4), 18% PEG 6000, and 0.5 M NaCl] and equilibrated against a 1 mL well reservoir of precipitant solution. Crystals appeared within 3−4 weeks and grew to maximal dimensions of 0.15 mm × 0.09 mm × 0.02 mm. X-ray diffraction data were collected from these crystals at beamline X29A at the Brookhaven National Synchrotron Light Source and processed to 2.2 Å resolution using the HKL suite of programs (*22*). Crystals belong to space group $P2_1$ with the following unit cell parameters: $a = 61.2$ Å, $b = 147.2$ Å, $c = 83.7$ Å, and $\beta = 97.9°$. With four molecules in the asymmetric unit, the Matthews coefficient $V_m = 2.6$ Å^3/Da, corresponding to a solvent content of 52%.

Initial phases for the electron density map of *A. terreus* aristolochene synthase were determined by molecular replacement using the structure of aristolochene synthase from *P. roqueforti* as a search probe for rotation and translation functions as implemented in Phaser 1.3 (*23*). After four monomers had been placed in the asymmetric unit, rigid-body refinement yielded R and R_{free} values of 0.460 and 0.457, respectively. Iterative rounds of refinement and model adjustment were performed using CNS (*24*) and O (*25*), respectively. Iterative cycles of refinement utilized torsion angle dynamics with a starting temperature of 5000 K in the initial stages of refinement with tight noncrystallographic symmetry (NCS) restraints relating the four monomers. With some differences among subunits being apparent, the NCS restraints were loosened as refinement progressed as guided by R_{free} and ultimately dropped for the last refinement cycles. The N-termini (M1−S12), C-termini (V318−D320), and loop segments of residues S231−G239 were disordered in all four monomers; thus, these residues are excluded from the final model. Continuous electron density peaks adjacent to five cysteine side chains were modeled as disulfide-linked BME molecules. Strong electron density peaks adjacent to R314 side chains in monomers B and C were interpreted as

[1] Abbreviations: PP_i, inorganic pyrophosphate; BME, β-mercaptoethanol; MES, 2-morpholinoethanesulfonic acid; NCS, noncrystallographic symmetry.

Table 1: Data Collection and Refinement Statistics

	unliganded enzyme	$Mg^{2+}{}_3$-PP_i complex
resolution range (Å)	50−2.20	50−2.15
no. of unique reflections >0 $\sigma(I)$	72129	70847
completeness (outer shell) (%)	94.9 (76.7)	90.5 (75.3)
overall $I/\sigma(I)$ (outer shell)	19.0 (2.3)	22.7 (2.1)
R_{merge} (outer shell)[a]	0.084 (0.534)	0.075 (0.650)
no. of protein atoms	9574	9625
no. of solvent atoms	191	238
no. of BME atoms	20	16
no. of chloride ions	2	0
no. of magnesium ions	0	3
no. of glycerol atoms	0	6
no. of MES atoms	12	0
no. of PP_i atoms	0	9
R_{cryst} (outer shell)[b]	0.222 (0.285)	0.229 (0.300)
R_{free} (outer shell)[b]	0.272 (0.330)	0.273 (0.340)
rms deviation		
bonds (Å)	0.007	0.008
angles (deg)	1.2	1.3
dihedral angles (deg)	19.0	19.2
improper dihedral angles (deg)	1.0	1.0

[a] $R_{merge} = \sum|I_i - \langle I_i\rangle|/\sum I_i$, where I_i is the observed intensity for reflection i and $\langle I_i\rangle$ is the average intensity calculated for reflection i from replicate data. [b] $R = \sum||F_o| - |F_c||/\sum|F_o|$, where R and R_{free} are calculated using the working and test reflection sets, respectively.

chloride ions. A large and continuous electron density peak in the active site cavity of monomer D was interpreted as a molecule of the buffer MES with its sulfonate group salt linked to the R314 side chain.

Individual thermal *B*-factors were refined, and refinement ultimately converged to a final crystallographic *R*-factor of 0.222 (R_{free} = 0.272) with excellent stereochemistry. Data collection and refinement statistics are summarized in Table 1. The buried surface area between monomers was calculated using the method of Lee and Richards with a 1.4 Å probe (*26*), as implemented in CNS (*24*).

The structure of *A. terreus* aristolochene synthase complexed with $Mg^{2+}{}_3$-PP_i was determined by soaking crystals of the native enzyme for 20 h in a buffer solution containing 100 mM Tris-HCl (pH 8.4), 18% PEG 6000, 0.5 M NaCl, 10 mM sodium pyrophosphate, 5 mM $MgCl_2$, and 5 mM benzyl tetraethyl ammonium chloride. X-ray diffraction data from these crystals were collected at the Cornell High Energy Synchrotron Source, beamline F-1, and processed to 2.15 Å resolution using the HKL suite of programs (*22*). Crystals were isomorphous with those of the native enzyme. The initial difference Fourier map revealed the binding of inorganic pyrophosphate and three Mg^{2+} ions to monomer D only. Significant conformational changes were evident in monomer D, and the polypeptide chain was rebuilt accordingly. Some attenuated conformational changes, but no ligand binding, were also observed in monomer C. Iterative rounds of refinement and model adjustment were performed using CNS (*24*) and O (*25*), respectively. The N-termini (M1−S12) and C-termini (V318−D320) were disordered in all four monomers, and the loop segments of residues S231−G239 were disordered in monomers A−C. The loop segment of residues N48−A51 was disordered in monomer C. The loop segment of residues S231−G239 was ordered in monomer D to accommodate the binding of $Mg^{2+}{}_3$-PP_i. Continuous electron density peaks adjacent to four cysteine side chains were modeled as disulfide-linked BME molecules. Individual thermal *B*-factors were refined, and a bulk solvent correction was applied. Refinement ultimately converged to a final crystallographic *R*-factor of 0.229 (R_{free} = 0.273) with excellent stereochemistry. Data collection and refinement statistics are summarized in Table 1. Molecular surfaces in the figures are calculated with Voidoo (*27*).

RESULTS

Aristolochene synthase from *A. terreus* adopts the α-helical class I terpene synthase fold (Figure 2a) first observed for avian farnesyl diphosphate synthase (*28*). There are a total of 13 α-helices, 6 of which surround the 20 Å deep active site cleft. Most of the helices are joined by short loops, approximately four or five residues in length. Two 10-residue loops connect helices D1 and E and helices F and G1, and a partly disordered 16-residue loop connects helices H and α-1. The aspartate-rich DDLLE motif beginning with D90 is located on the C-terminal end of helix D on the upper wall of the active site cleft, and the NSE/DTE motif starting with V217 is located on helix H on the opposite wall of the active site cleft. No metal ions are observed bound to these motifs in the structure of the unliganded enzyme.

Aristolochene synthase from *A. terreus* is reported to be a monomer in solution on the basis of the results of gel filtration chromatography (*16*). However, native gel analysis indicates dimeric quaternary structure (Figure 3), and the crystal structure reveals the assembly of two dimers in the asymmetric unit that form a tetramer with 222 point group symmetry (Figure 2b,c). This is the first example of tetrameric quaternary structure in the greater family of terpenoid cyclases. The total surface areas of individual monomers and the buried surface areas between monomers are presented in Table 2. The AD and BC monomer pairs are each related by noncrystallographic symmetry and form the largest interface with an average buried surface area of 1634 Å^2. This interface is enriched with numerous hydrophobic side chains, as well as polar residues (E251, E259, D253, and R273) that form direct and solvent-mediated intersubunit hydrogen bonds. The AC and BD monomer pairs each form a significant, somewhat polar interface with an average buried surface area of 1009 Å^2. Finally, the AB and CD monomer pairs bury an average of 720 Å^2 of polar and nonpolar surface area. In total, each monomer buries approximately 23% of its total surface area upon tetramer formation, which corresponds to the average buried surface area of 23% per subunit said to characterize homotetramer assembly (*29*). Therefore, we conclude that *A. terreus* aristolochene synthase likely functions as the AD or BC dimer in solution, but it is capable of oligomerization at higher enzyme concentrations to form a tetramer.

Such oligomerization may be responsible for the previously documented attenuation of enzyme activity at enzyme concentrations greater than 27 nM (*21*), e.g., by hindering conformational changes required for catalysis. In light of this observation, it is intriguing that although the structure of *A. terreus* aristolochene synthase complexed with $Mg^{2+}{}_3$-PP_i is the first structure of a ligand complex with an aristolochene synthase from any species, the $Mg^{2+}{}_3$-PP_i cluster binds only to subunit D of the tetramer (Figure 4a). Furthermore, X-ray crystallographic analysis of enzyme crystals soaked in

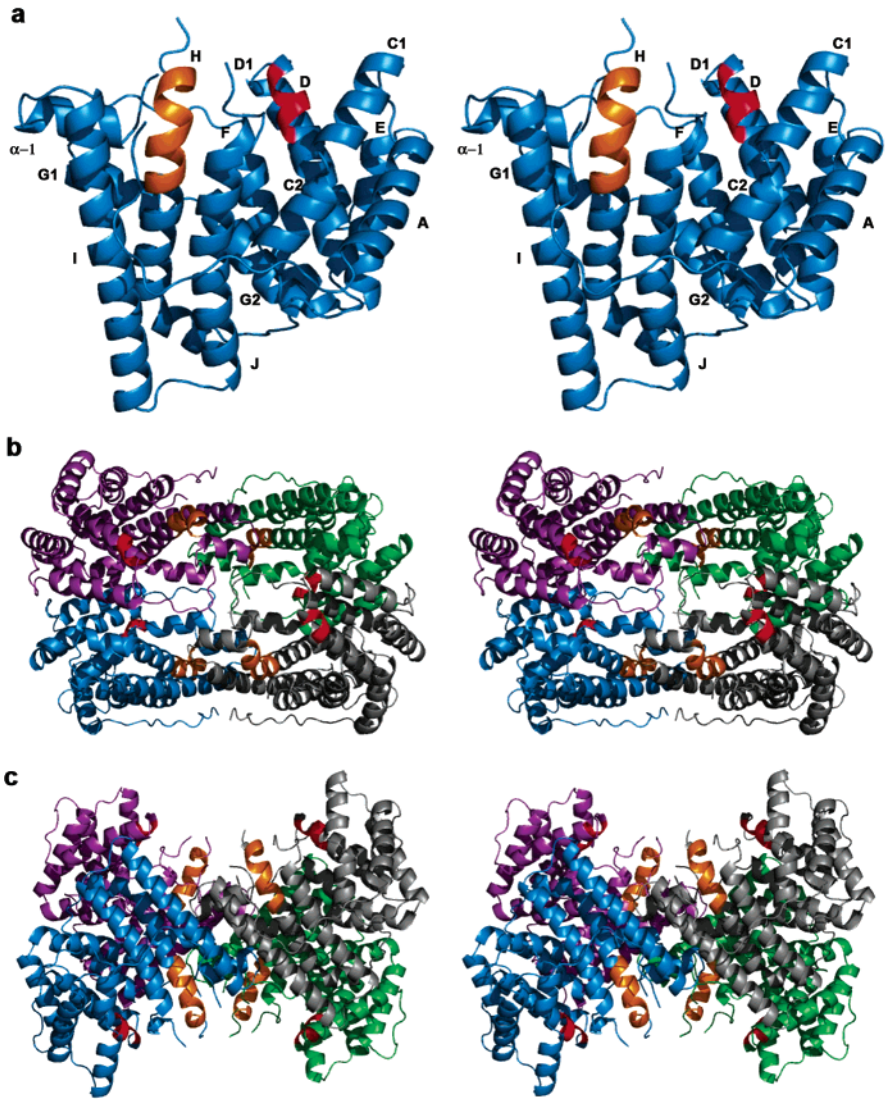

FIGURE 2: Ribbon plots of *A. terreus* aristolochene synthase. (a) Stereoview of cyclase monomer A showing the aspartate-rich motif (red) and the aspartate-poor NSE/DTE motif (orange) flanking the mouth of the active site. Helices are labeled according to the convention first established for farnesyl diphosphate synthase (*28*). (b) Cyclase monomers A (blue), B (green), C (purple), and D (gray) assemble to form a dimer of dimers. (c) Same as panel b but rotated by 90°.

solutions containing farnesyl diphosphate reveals the binding of intact substrate molecules in the active sites of monomers A−C and just PP_i in the active site of monomer D (study in progress). Accordingly, substrate-induced conformational changes required for active site closure and catalysis may indeed be hindered in monomers A−C of the tetramer.

In the aristolochene synthase−Mg^{2+}_3-PP_i complex, the carboxylate of D90 (the first residue of the aspartate-rich motif on helix D) coordinates to Mg^{2+}_A and Mg^{2+}_C with syn,-syn-bidentate geometry. No other residues in the aspartate-rich motif participate in metal binding: D91 makes a salt bridge interaction with R314, and D94 accepts hydrogen bonds from water molecules 1 (coordinated to Mg^{2+}_A) and 66. In addition to D90, five other ligands coordinate to Mg^{2+}_A, including the PP_i anion and four water molecules (molecules 4 and 70−72). The Mg^{2+}_C ion is coordinated by D90, PP_i, and water molecules 1, 3, and 70. Adjacent to the Mg^{2+}_3-PP_i cluster is a glycerol molecule that makes hydrogen bond interactions with metal-coordinated water molecules 4 and 70. In the NSE/DTE motif, N219, S223, and E227 coordinate to Mg^{2+}_B in a fashion identical to that observed in other terpenoid cyclases such as 5-epi-aristolochene synthase (*11*), trichodiene synthase (*14*), and bornyl diphosphate synthase (*30*).

In addition to multiple metal coordination interactions, the PP_i anion accepts hydrogen bonds from basic residues R175, K226, R314, and also Y315 (Figure 4b). These residues are analogous to R182, K232, R304, and Y305 of trichodiene synthase and make an identical constellation of interactions with PP_i (Figure 4c) (*14*). It is remarkable that despite the massive evolutionary drift separating these two different fungal cyclases related by only a 15% level of amino acid sequence identity, the molecular recognition of Mg^{2+}_3-PP_i and the substrate diphosphate group is perfectly conserved.

It is interesting to note the interaction between D91 (the second aspartate residue in the aspartate-rich motif) and R314, which also donates a hydrogen bond to PP_i. In the active sites of other terpenoid cyclases, the second aspartate in the aspartate-rich DDXXD/E motif typically interacts with an arginine residue located on a neighboring helix. For example, D352 in the aspartate-rich motif of bornyl diphosphate synthase accepts a hydrogen bond from R314, which

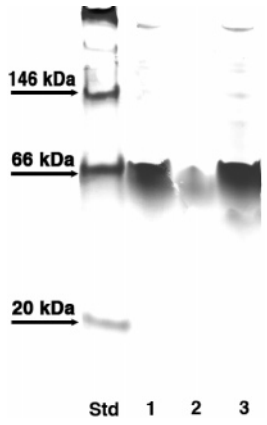

FIGURE 3: Native gel analysis of *A. terreus* aristolochene synthase oligomerization in solution. Novex Tris-glycine sample native buffer was added to 28 μM, 20 nM, and 11 mM enzyme in 25 mM MES (pH 6.5), 2 mM $MgCl_2$, 0.15 M NaCl, and 4 mM BME. The NativeMark Unstained protein standard from Invitrogen and enzyme samples were electrophoresed on a 10 to 20% native Tris-glycine gel at 125 V and 4 °C in 50 mM Tris-glycine buffer (pH 8.8) for approximately 5 h. Lanes labeled 1−3 contained 28 μM, 20 nM, and 11 mM aristolochene synthase, respectively. The native enzyme migrates as an ∼70 kDa dimer.

Table 2: Surface Areas of Individual Monomers and Buried Surface Areas upon Tetramer Formation

		buried surface area upon tetramer formation (Å^2)			
monomer	total surface area (Å^2)	A	B	C	D
A	14 804		786	1088	1632
B	14 848	786		1636	930
C	14 872	1088	1636		653
D	14 490	1632	930	653	

in turn donates a hydrogen bond to the PP_i anion in the $Mg^{2+}{}_3$-PP_i complex (*30*). In trichodiene synthase, D101 of the aspartate-rich motif accepts a hydrogen bond from R304, which in turn donates a hydrogen bond to the PP_i anion in the $Mg^{2+}{}_3$-PP_i complex (Figure 4c) (*14*). In addition to protein−metal ion−diphosphate interactions, aspartate−arginine−diphosphate interactions in the greater family of terpene cyclases provide the substrate with a direct connection to trigger and control protein structural changes required for the transition of the cyclase active site from the solvent-exposed open conformation to the solvent-sequestered closed conformation (Figure 4d).

The binding of $Mg^{2+}{}_3$-PP_i to monomer D of *A. terreus* aristolochene synthase triggers significant conformational changes such that the rms deviation of 300 Cα atoms between the unliganded and liganded structures is 1.8 Å. The most significant changes are observed in helices G1 and H, in the N-terminus, and in the F−G1 loop (Figure 4d). The N-terminal portion of the H−α1 loop is incorporated into an extension of helix H; helices C1, D1, F, G1, and H shift inward, and the previously disordered H−α1 loop (S231−G239) adopts a well-defined conformation that caps the active site. Other secondary structural elements that undergo significant movement include helices D, F, and I. These conformational changes are likely to be triggered as well by the diphosphate group of the substrate, farnesyl diphosphate, thereby bringing ligand-binding residues closer together and simultaneously sequestering the active site from bulk solvent. These conformational changes must also trigger the ionization of the substrate diphosphate group to initiate the cyclization cascade summarized in Figure 1.

DISCUSSION

It is notable that aristolochene synthases from *A. terreus* and *P. roqueforti* divergently evolved yet preserved the ability to cyclize farnesyl diphosphate to form the same hydrocarbon product with exquisite structural and stereochemical precision. Although the *P. roqueforti* aristolochene synthase also produces minor amounts of the intermediate germacrene A and the side product valencene (4 and 2%, respectively), the *A. terreus* enzyme produces aristolochene as the single sesquiterpene product (*21*). Of course, the substitution of active site residues important for metal binding can significantly compromise catalysis and cyclization fidelity in both cyclases (*21*). Mutagenesis and structural studies of the related sesquiterpene cyclase trichodiene synthase demonstrate that slight alterations in a metal binding site, e.g., the substitution of a glutamate ligand for an aspartate ligand in the aspartate-rich motif (*31*, *32*), or the substitution of polar residues that donate hydrogen bonds to the substrate diphosphate group (*33*−*36*), can alter the active site contour in the catalytically active closed conformation of the cyclase sufficiently to compromise catalytic efficiency and/or lead to the formation of aberrant cyclization products. How, then, are the amino acid substitutions between aristolochene synthases from *A. terreus* and *P. roqueforti* (61% identical sequences) accommodated so that the structural and stereochemical precision of aristolochene biosynthesis is preserved?

The overall fold of the aristolochene synthase monomer from *A. terreus* is similar to that of *P. roqueforti* (Figure 5a), and the root-mean-square (rms) deviation between the two structures is 1.0 Å for 282 Cα atoms. The majority of amino acid substitutions between the two enzymes are found on the protein surfaces (Figure 5b), although several are located within the interior of the protein. To some extent, the protein structures compensate for interior amino acid substitutions to preserve the overall fold (Figure 5a), either by adjustments of surrounding residues to accommodate changes in the volume and shape of mutated side chains or by rearrangements of hydrogen bond networks. Importantly, most of the residues lining the active site clefts are highly conserved between the two enzymes so that the active site contours are remarkably similar (Figure 6a,b). Although there is an only modest level of amino acid sequence identity between the H−α1 loop segments that cap the active sites in the two aristolochene synthases (*A. terreus*, Y^{229}-TSKTAHSEGGI; *P. roqueforti*, E^{254}ASRTGHKEGAF), the key residues are conserved. Thus, K232 in the *A. terreus* enzyme, which interacts with the bound PP_i moiety, corresponds to R257 in the *P. roqueforti* enzyme.

In contrast, the active site contours of trichodiene synthase and 5-epi-aristolochene synthase, enzymes that generate structurally and/or stereochemically different products, are strikingly different from one another as well as from the contours of the two aristolochene synthases (Figure 6c,d). Comparison of all the active site contours illustrated in Figure 6 validates the template function postulated for the

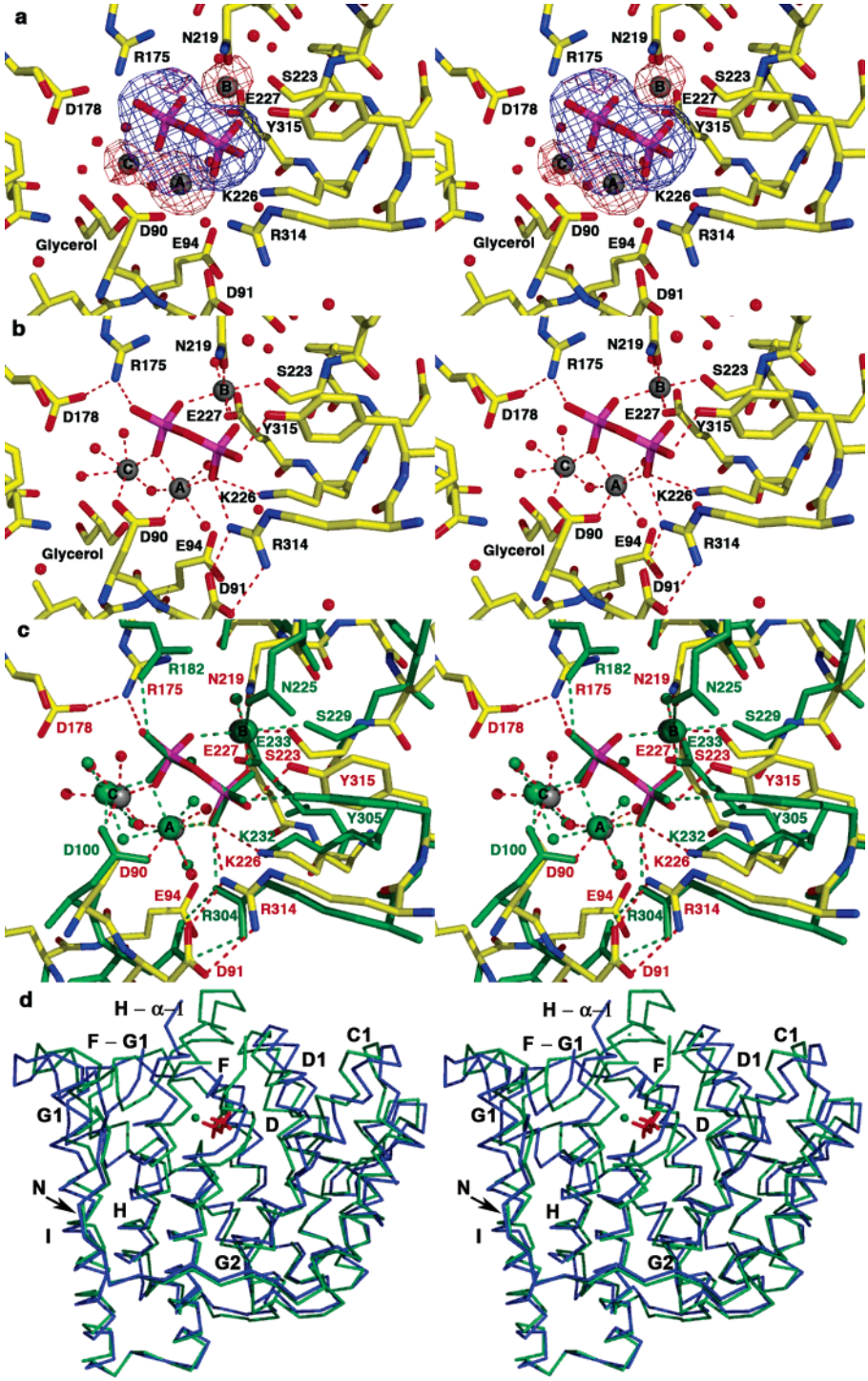

FIGURE 4: Aristolochene synthase−$Mg^{2+}{}_3$-PP_i complex. (a) Simulated annealing omit maps of the PP_i anion (blue) and Mg^{2+} ions (red) contoured at 3σ. The Mg^{2+} ions are shown as gray spheres and water molecules as red spheres. (b) Same orientation as panel a showing selected metal coordination and hydrogen bond interactions. (c) Superposition of aristolochene synthase and trichodiene synthase (green) active sites in their $Mg^{2+}{}_3$-PP_i complexes. (d) Least-squares superposition of 300 Cα atoms between unliganded (blue) and $Mg^{2+}{}_3$-complexed (green) aristolochene synthase. Glycerol molecules are omitted from both structures for clarity. Significant conformational changes are triggered in the indicated helices and loops by $Mg^{2+}{}_3$-PP_i binding.

terpene cyclase active site, in which a unique surface contour enforces the precise conformation of farnesyl diphosphate required for cyclization to form a unique product. Furthermore, the template is quite complementary in shape to the cyclization product, as shown in Figure 7 for *A. terreus* aristolochene synthase. Interestingly, the cyclization template is defined by a handful of conserved residues in aristolochene synthases from *A. terreus* and *P. roqueforti*, whereas the corresponding residues have largely diverged in trichodiene synthase and pentalenene synthase. The highly variable evolutionary fate of active site residues defining the cyclization template is consistent with their designation as "plasticity residues" by Keasling and colleagues (*37*), who elegantly demonstrate that a single terpene cyclase active site can serve as a highly evolvable template for the synthesis of cyclic hydrocarbons with diverse structures and stereochemistries.

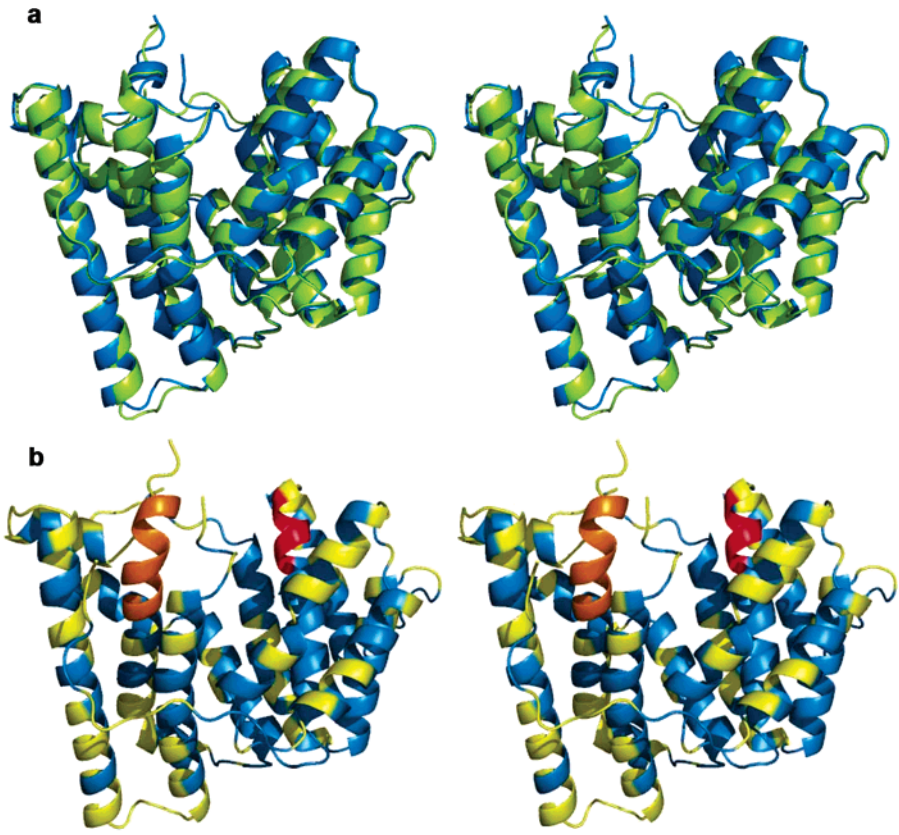

FIGURE 5: (a) Superposition of aristolochene synthases from *A. terreus* (blue) and *P. roqueforti* (green). Aristolochene synthase from *P. roqueforti* crystallizes as a dimer along a 2-fold noncrystallographic axis. With a buried surface area of 1630 Å^2, the dimer interface is identical to those between the AD and BC monomer pairs in the *A. terreus* enzyme. (b) Stereoview of aristolochene synthase from *A. terreus* with sites of amino acid substitutions in the *P. roqueforti* enzyme colored yellow. Aspartate-rich and NSE/DTE motifs are colored red and orange, respectively.

One could argue that the active site surface contour of a terpenoid cyclase is different in the open, unliganded state compared with the closed, ligand-bound state. However, despite the obvious changes in the contour of the upper active site triggered by its closure, the salient features of the lower active site surface contour appear to be preserved in both the open and closed conformations of *A. terreus* aristolochene synthase (Figure 7). Furthermore, the cyclization product is unambiguously modeled into the active site surface contour of the closed conformation (Figure 7). Since the unique characteristics of the template are largely conserved in closed and open conformations, it is possible that the cyclization product of a terpenoid cyclase might ultimately be predicted or engineered solely on the basis of the analysis of the three-dimensional contour of its active site in either conformation.

Given the similar active site contours of aristolochene synthases from *A. terreus* and *P. roqueforti*, the structural analysis and mechanistic implications discussed by Caruthers and colleagues (*13*) for the *P. roqueforti* enzyme are directly relevant to the *A. terreus* enzyme. Specifically, aromatic residues F112, F178, and W334 of the *P. roqueforti* enzyme appear to be appropriately oriented to stabilize sites of developing partial positive charge as well as carbocation intermediates in catalysis. These residues are conserved in the *A. terreus* enzyme as F87, F153, and W308, respectively. The results of site-directed mutagenesis experiments suggest that W334 of the *P. roqueforti* enzyme and W308 of the *A. terreus* enzyme stabilize the eudesmane cation (*38*). Electrostatic stabilization of highly reactive carbocation intermediates through cation$-\pi$ interactions (*39*, *40*) is a catalytic strategy adopted by all terpenoid cyclases (*9*). Additionally, just as the active site contour of the *P. roqueforti* enzyme is well-suited for the binding of the eudesmane cation (Figure 1) with a *trans*-decalin configuration, so too is the active site of the *A. terreus* enzyme due to their similar active site contours (Figure 6a,b). The active site of 5-epi-aristolochene synthase must accommodate the *cis*-decalin configuration of the eudesmane cation with a significantly different active site contour (Figure 6c).

The phenolic side chain of Y92 in *P. roqueforti* aristolochene synthase, conserved as Y67 in the *A. terreus* enzyme, was initially hypothesized to be the active site general acid/base responsible for the protonation of the germacrene A intermediate and the deprotonation of the eudesmane cation (Figure 1) (*13*). However, site-directed mutagenesis experiments with Y92F aristolochene synthase from *P. roqueforti* reveal the generation of appreciable quantities of aristolochene (*21*, *41*, *42*). Therefore, neither Y92 of the *P. roqueforti* enzyme nor Y67 of the *A. terreus* enzyme can be the catalytically obligatory general acid/base. Since the product aristolochene fits so precisely into the active site cavity in the closed conformation (Figure 7), it is unlikely that a solvent molecule could be trapped in the enclosed active site to perform a general acid/base function. Therefore, on the basis of the inspection of the structure of the $Mg^{2+}{}_3$-PP_i complex, we propose that the PP_i moiety is the best candidate for the general acid/base.

Specifically, consider the deprotonation of C8-H_β in the eudesmane cation (Figure 1). The O3 and O6 atoms of PP_i are oriented into the active site cavity; on the basis of a

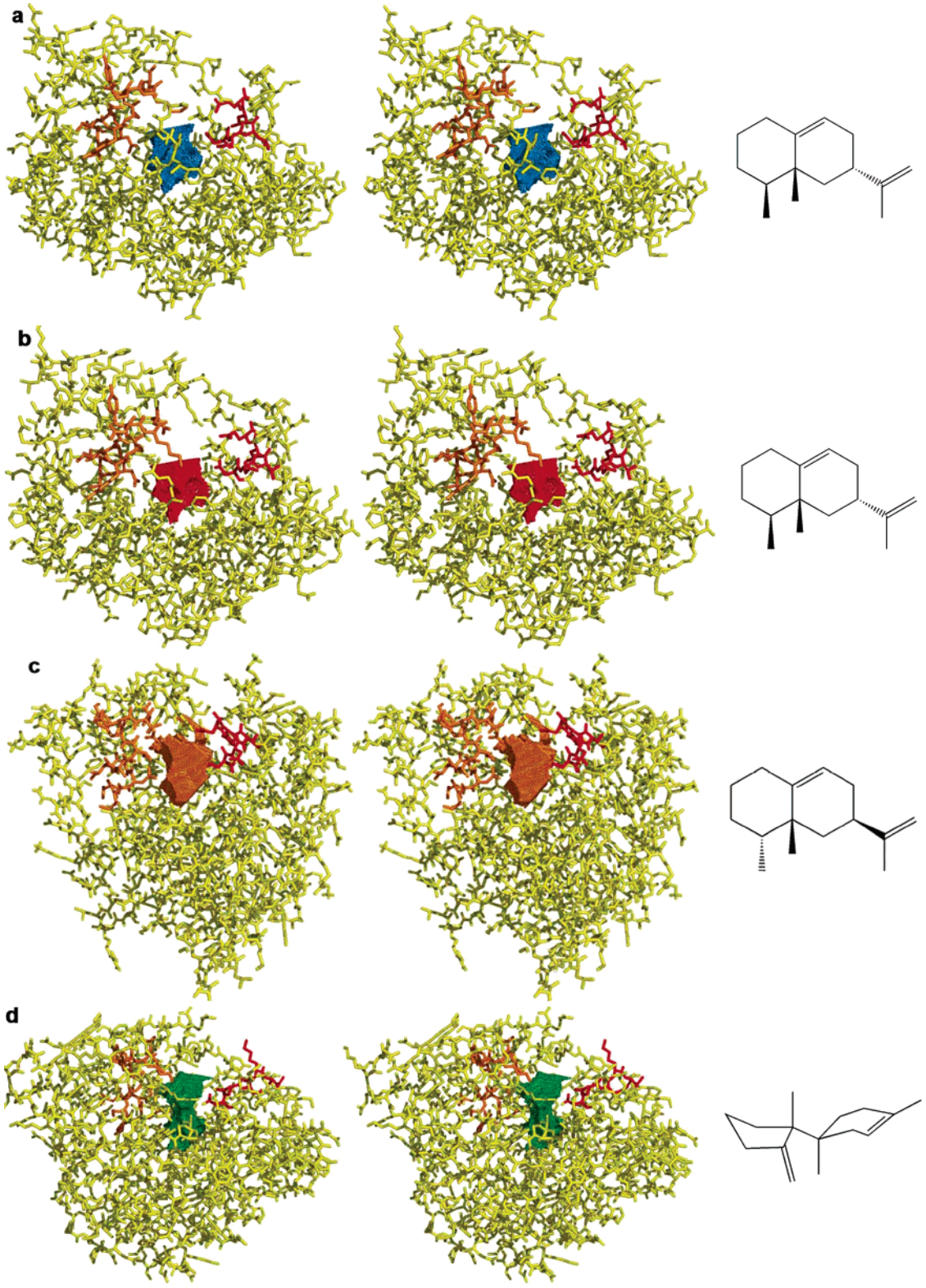

FIGURE 6: Stereoviews of sesquiterpene cyclases and their solvent accessible active site surface contours in the open, unliganded conformations: (a) aristolochene synthase from *A. terreus*, (b) aristolochene synthase from *P. roqueforti*, (c) C-terminal domain of 5-epi-aristolochene synthase, and (d) trichodiene synthase. Aspartate-rich motifs (red) and NSE/DTE motifs (orange) indicate the comparable orientations of active site clefts, roughly comparable to that shown in Figure 2a for aristolochene synthase from *A. terreus*. Shown at the right are the cyclic sesquiterpenes generated by each enzyme.

comparison with trichodiene synthase (*36*) and bornyl diphosphate synthase (*30*), the O6 atom corresponds to the phosphoester oxygen and the O3 atom corresponds to the terminal phosphate group of the substrate farnesyl diphosphate. In the aristolochene synthase complex with $Mg^{2+}{}_3$-PP_i, the O3 and O6 atoms of PP_i are 3.2 and 4.6 Å, respectively, from the aristolochene C8 atom when the product is modeled into its complementary surface contour (Figure 7). If the bicyclic eudesmane cation binds in a position and orientation comparable to that modeled for the

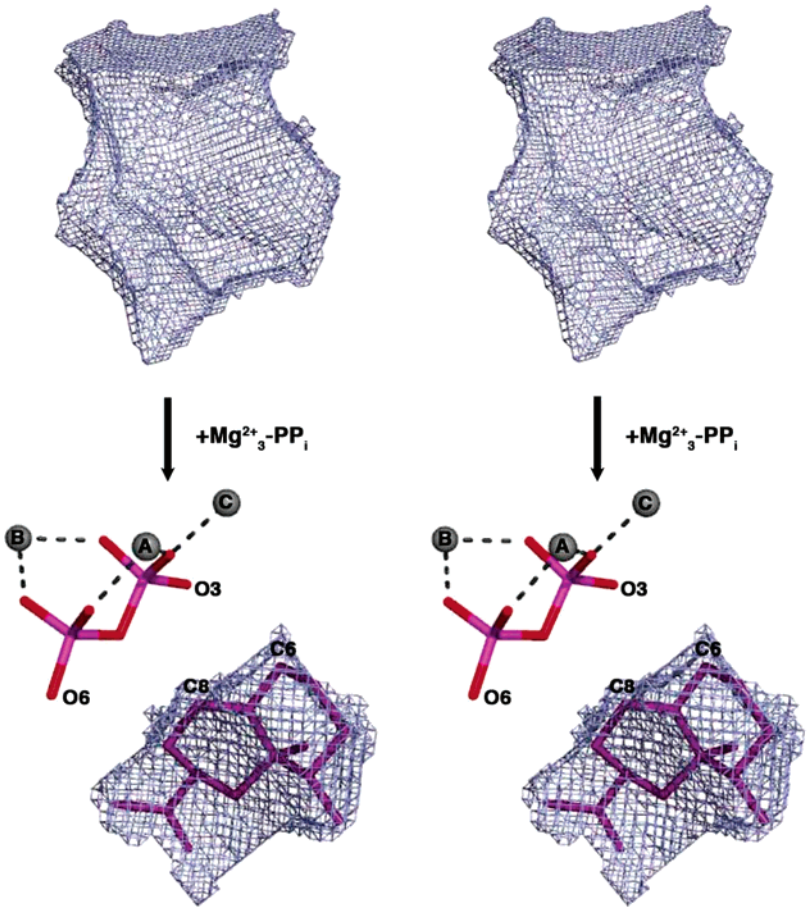

FIGURE 7: Active site surface contours of *A. terreus* aristolochene synthase in the unliganded (from Figure 6a) and liganded (closed) conformation. The cyclization product, (+)-aristolochene, is modeled into the active site of the closed conformation, and the location of the $Mg^{2+}{}_3$-PP_i cluster is shown as a visual reference. The unique template required for the cyclization of farnesyl diphosphate is preserved in the lower active site contour in both open and closed conformations. The O6 atom of PP_i corresponds to the original phosphoester oxygen, and the O3 atom corresponds to the terminal phosphate group of the substrate, farnesyl diphosphate. The proximity of the PP_i O3 atom to aristolochene C6 and C8 atoms (3.4 and 3.2 Å, respectively) implicates PP_i as the general acid/general base illustrated in Figure 1.

bicyclic product, the O3 atom of PP_i would be properly oriented for the stereospecific deprotonation of C8-H_β in the eudesmane cation.

In the preceding step, the conjugate acid of PP_i could protonate the intermediate germacrene A at C6 to generate the eudesmane cation in the preceding step (Figure 1), since the O3 atom of PP_i is also 3.4 Å from the corresponding atom of aristolochene when the product is modeled into its complementary surface contour (Figure 7). However, the origin of such a proton might be unclear. Experiments with [12,12,12-$^2H_3$]farnesyl diphosphate (*18*) do not indicate any return of the original deuterium to C6 in the protonation of germacrene A, suggesting that the substrate deprotonation in the first step of the cyclization reaction does not involve the single general acid/general base invoked in Figure 1 unless there is competing rapid exchange of the PP_i-bound proton with the external medium, e.g., across metal-bound solvent molecules observed in the $Mg^{2+}{}_3$-PP_i complex. It is conceivable that following ionization of farnesyl diphosphate, O6 of the newly generated $Mg^{2+}{}_3$-PP_i complex deprotonates the paired germacradienyl cation, with the distal O3 atom of the PP_i then donating a different proton to C6 of the intermediate germacrene A.

Although we previously speculated that the PP_i anion might be involved in catalysis of the cyclization reaction, on the basis of analysis of the structure of unliganded aristolochene synthase from *P. roqueforti* (*13*), the structure of *A. terreus* aristolochene synthase complexed with $Mg^{2+}{}_3$-PP_i provides the first structural evidence that the PP_i anion is indeed positioned and oriented to function as a possible general acid/general base for catalysis. This function is comparable to that recently proposed for the PP_i anion in the termination step of the cationic chain elongation reaction catalyzed by farnesyl diphosphate synthase (*43*). Accordingly, aristolochene synthase may do relatively little in catalysis other than to fold the substrate farnesyl diphosphate into a suitable conformation and then trigger substrate ionization, while providing a solvent-shielded template for the ensuing cyclization cascade and allowing for substrate-assisted catalysis by the pyrophosphate leaving group. Consistent with such a catalytic strategy, it is notable that the slowest chemical step in sesquiterpene cyclization reactions is typically the ionization of the farnesyl diphosphate substrate ($1-5\ s^{-1}$), with all subsequent cyclizations, rearrangements, and deprotonations occurring as much as 100 times more rapidly ($>200\ s^{-1}$) (*44*, *45*). It is intriguing to speculate that such a catalytic strategy may be widespread among the greater family of terpenoid cyclases.

ACKNOWLEDGMENT

We thank the National Synchrotron Light Source at Brookhaven National Laboratory for access to X-ray crystallographic data collection facilities at beamline X29A and the Cornell High Energy Synchrotron Source for access to beamline F-1. We also thank L. Sangeetha Vedula for helpful advice.

REFERENCES

1. Glasby, J. S. (1982) *Encyclopedia of Terpenoids*, Wiley, Chichester, U.K.
2. Pichersky, E., Noel, J. P., and Dudareva, N. (2006) Biosynthesis of plant volatiles: Nature's diversity and ingenuity, *Science 311*, 808−811.
3. Cane, D. E. (1985) Isoprenoid biosynthesis. Stereochemistry of the cyclization of allylic pyrophosphates, *Acc. Chem. Res. 18*, 220−226.
4. Cane, D. E. (1990) Enzymatic formation of sesquiterpenes, *Chem. Rev. 90*, 1089−1103.
5. Lesburg, C. A., Caruthers, J. M., Paschall, C. M., and Christianson, D. W. (1998) Managing and manipulating carbocations in biology: Terpenoid cyclase structure and mechanism, *Curr. Opin. Struct. Biol. 8*, 695−703.
6. Wendt, K. U., and Schulz, G. E. (1998) Isoprenoid biosynthesis: Manifold chemistry catalyzed by similar enzymes, *Structure 6*, 127−133.
7. Wise, M. L., and Croteau, R. (1999) Monoterpene biosynthesis, in *Comprehensive Natural Products Chemistry: Isoprenoids Including Carotenoids and Steroids* (Cane, D. E., Ed.) Vol. 2, pp 97−153, Elsevier, Oxford, U.K.
8. Cane, D. E. (1999) Sesquiterpene biosynthesis: Cyclization mechanisms, in *Comprehensive Natural Products Chemistry: Isoprenoids Including Carotenoids and Steroids* (Cane, D. E., Ed.) Vol. 2, pp 155−200, Elsevier, Oxford, U.K.
9. Christianson, D. W. (2006) Structural biology and chemistry of the terpenoid cyclases, *Chem. Rev. 106*, 3412−3442.
10. Steele, C. L., Crock, J., Bohlmann, J., and Croteau, R. (1998) Sesquiterpene synthases from Grand fir (*Abies grandis*). Comparison of constitutive and wound-induced activities, and cDNA isolation, characterization, and bacterial expression of δ-selinene synthase and γ-humulene synthase, *J. Biol. Chem. 273*, 2078−2089.
11. Starks, C. M., Back, K., Chappell, J., and Noel, J. P. (1997) Structural basis for cyclic terpene biosynthesis by tobacco 5-epi-aristolochene synthase, *Science 277*, 1815−1820.
12. Lesburg, C. A., Zhai, G., Cane, D. E., and Christianson, D. W. (1997) Crystal structure of pentalenene synthase: Mechanistic insights on terpenoid cyclization reactions in biology, *Science 277*, 1820−1824.
13. Caruthers, J. M., Kang, I., Rynkiewicz, M. J., Cane, D. E., and Christianson, D. W. (2000) Crystal structure determination of aristolochene synthase from blue cheese mold, *Penicillium roqueforti*, *J. Biol. Chem. 275*, 25533−25539.
14. Rynkiewicz, M. J., Cane, D. E., and Christianson, D. W. (2001) Structure of trichodiene synthase from *Fusarium sporotrichioides* provides mechanistic inferences on the terpene cyclization cascade, *Proc. Natl. Acad. Sci. U.S.A. 98*, 13543−13548.
15. Ashby, M. N., and Edwards, P. A. (1990) Elucidation of the deficiency in two yeast coenzyme Q mutants. Characterization of the structural gene encoding hexaprenyl pyrophosphate synthetase, *J. Biol. Chem. 265*, 13157−13164.
16. Cane, D. E., and Kang, I. (2000) Aristolochene synthase: Purification, molecular cloning, high-level expression in *Escherichia coli*, and characterization of the *Aspergillus terreus* cyclase, *Arch. Biochem. Biophys. 376*, 354−364.
17. Cane, D. E., Prabhakaran, P. C., Salaski, E. J., Harrison, P. H. M., Noguchi, H., and Rawlings, B. J. (1989) Aristolochene biosynthesis and enzymatic cyclization of farnesyl pyrophosphate, *J. Am. Chem. Soc. 111*, 8914−8916.
18. Cane, D. E., Prabhakaran, P. C., Oliver, J. S., and McIlwaine, D. B. (1990) Aristolochene biosynthesis. Stereochemistry of the deprotonation steps in the enzymatic cyclization of farnesyl pyrophosphate, *J. Am. Chem. Soc. 112*, 3209−3210.
19. Cane, D. E., and Tsantrizos, Y. S. (1996) Aristolochene synthase. Elucidation of the cryptic germacrene A synthase activity using the anomalous substrate dihydrofarnesyl diphosphate, *J. Am. Chem. Soc. 118*, 10037−10040.
20. Cane, D. E., and Bryant, C. (1994) Aristolochene synthase. Mechanism-based inhibition of a terpenoid cyclase, *J. Am. Chem. Soc. 116*, 12063−12064.
21. Felicetti, B., and Cane, D. E. (2004) Aristolochene synthase: Mechanistic analysis of active site residues by site-directed mutagenesis, *J. Am. Chem. Soc. 126*, 7212−7221.
22. Otwinowski, Z., and Minor, W. (1997) Processing of X-ray diffraction data collected in oscillation mode, *Methods Enzymol. 276*, 306−326.
23. McCoy, A. J., Grosse-Kunstleve, R. W., Storoni, L. C., and Read, R. J. (2005) Likelyhood-enhanced fast translation functions, *Acta Crystallogr. D61*, 458−464.
24. Brünger, A. T., Adams, P. D., Clore, G. M., DeLano, W. L., Gros, P., Grosse-Kunstleve, R. W., Jiang, J.-S., Kuszewski, J., Nilges, M., Pannu, N. S., Read, R. J., Rice, L. M., Simonson, T., and Warren, G. L. (1998) Crystallography and NMR system: A new software suite for macromolecular structure determination, *Acta Crystallogr. D54*, 905−921.
25. Jones, T. A., Zou, J.-Y., Cowan, S. W., and Kjeldgaard, M. (1991) Improved methods for building protein models in electron density maps and the location of errors in these models, *Acta Crystallogr. A47*, 110−119.
26. Lee, B., and Richards, F. M. (1971) The interpretation of protein structures: Estimation of static accessibility, *J. Mol. Biol. 55*, 379−400.
27. Kleywegt, G. J., and Jones, T. A. (1994) Detection, delineation, measurement and display of cavities in macromolecular structures, *Acta Crystallogr. D50*, 178−185.
28. Tarshis, L. C., Yan, M., Poulter, D., and Sacchettini, J. C. (1994) Crystal structure of recombinant farnesyl diphosphate synthase at 2.6-Å resolution, *Biochemistry 33*, 10871−10877.
29. Ponstingl, H., Kabir, T., Gorse, D., and Thornton, J. M. (2005) Morphological aspects of oligomeric protein structures, *Prog. Biophys. Mol. Biol. 89*, 9−35.
30. Whittington, D. A., Wise, M. L., Urbansky, M., Coates, R. M., Croteau, R. B., and Christianson, D. W. (2002) Bornyl diphosphate synthase: structure and strategy for carbocation manipulation by a terpenoid cyclase, *Proc. Natl. Acad. Sci. U.S.A. 99*, 15375−15380.
31. Cane, D. E., Xue, Q., and Fitzsimons, B. C. (1996) Trichodiene synthase. Probing the role of the highly conserved aspartate-rich region by site-directed mutagenesis, *Biochemistry 35*, 12369−12376.
32. Rynkiewicz, M. J., Cane, D. E., and Christianson, D. W. (2002) X-ray crystal structures of D100E trichodiene synthase and its pyrophosphate complex reveal the basis for terpene product diversity, *Biochemistry 41*, 1732−1741.
33. Cane, D. E., Shim, J. H., Xue, Q., and Fitzsimons, B. C. (1995) Trichodiene synthase. Identification of active site residues by site-directed mutagenesis, *Biochemistry 34*, 2480−2488.
34. Cane, D. E., and Xue, Q. (1996) Trichodiene synthase. Enzymatic formation of multiple sesquiterpenes by alteration of the cyclase active site, *J. Am. Chem. Soc. 118*, 1563−1564.
35. Vedula, L. S., Rynkiewicz, M. J., Pyun, H.-J., Coates, R. M., Cane, D. E., and Christianson, D. W. (2005) Molecular recognition of the substrate diphosphate group governs product diversity in trichodiene synthase mutants, *Biochemistry 44*, 6153−6163.
36. Vedula, L. S., Cane, D. E., and Christianson, D. W. (2005) Role of arginine-304 in the diphosphate-triggered active site closure mechanism of trichodiene synthase, *Biochemistry 44*, 12719−12727.
37. Yoshikuni, Y., Ferrin, T. E., and Keasling, J. D. (2006) Designed divergent evolution of enzyme function, *Nature 440*, 1078−1082.
38. Deligeorgopoulou, A., Taylor, S. E., Forcat, S., and Allemann, R. K. (2003) Stabilisation of eudesmane cation by tryptophan 334 during aristolochene synthase catalysis, *Chem. Commun. 17*, 2162−2163.
39. Dougherty, D. A. (1996) Cation-π interactions in chemistry and biology: A new view of benzene, Phe, Tyr, and Trp, *Science 271*, 163−168.
40. Jenson, C., and Jorgensen, W. L. (1997) Computational investigations of carbenium ion reactions relevant to sterol biosynthesis, *J. Am. Chem. Soc. 119*, 10846−10854.

41. Calvert, M. J., Ashton, P. R., and Allemann, R. K. (2002) Germacrene A is a product of the aristolochene synthase-mediated conversion of farnesyl pyrophosphate to aristolochene, *J. Am. Chem. Soc. 124*, 11636−11641.
42. Deligeorgopoulou, A., and Allemann, R. K. (2003) Evidence for differential folding of farnesyl pyrophosphate in the active site of aristolochene synthase: A single-point mutation converts aristolochene synthase into an (*E*)-β-farnesene synthase, *Biochemistry 42*, 7741−7747.
43. Hosfield, D. J., Zhang, Y., Dougan, D. R., Broun, A., Tari, L. W., Swanson, R. V., and Finn, J. (2004) Structural basis for bisphosphonate-mediated inhibition of isoprenoid biosynthesis, *J. Biol. Chem. 279*, 8526−8529.
44. Cane, D. E., Chiu, H.-T., Liang, P.-H., and Anderson, K. S. (1997) Pre-steady-state kinetic analysis of the trichodiene synthase reaction pathway, *Biochemistry 36*, 8332−8339.
45. Mathis, J. R., Back, K., Starks, C., Noel, J., Poulter, C. D., and Chappell, J. (1997) Pre-steady-state study of recombinant sesquiterpene cyclases, *Biochemistry 36*, 8340−8348.

BI0622524